

Radiometric Performance of Digital Image Data Collection - A Comparison of ADS40/DMC/UltraCam and EmergeDSS

EIJA HONKAVAARA, LAURI MARKELIN, Helsinki

ABSTRACT

The digital photogrammetric sensors offer attractive radiometric properties, including linearity of the radiometric response, large dynamic range, great radiometric resolution, low noise level, and multi-spectral and multiangular imagery. Radiometric processing chains should be developed for the photogrammetric production lines in order to utilize these properties into optimum effect and to ensure the usability of the data as historical data sets in the future. The resulting data can be applied in conventional photogrammetric tasks as well as in automated image interpretation applications, such as change detection and classification.

In this study the radiometric properties of digital large format sensors ADS40, DMC, and UltraCamD and the medium format Emerge DSS were studied from the available literature and using empirical image data sets. The radiometry of the DSS was optimized for visual interpretation, thus the analysis is not quite comparable to the analysis of the large format sensors. Literature describes various sensors in different details. The empirical study proved quantitatively the above enumerated radiometric properties. Detected problems included the low sensitivity of the ADS40 multispectral channels and the risk of overexposure of the UltraCamD and DMC in certain conditions and system configuration. The results showed that the airborne system characterization is necessary. Different sensor designs provide different spectral and radiometric properties and potential, and the future studies will show the applicability of the sensors for various applications.

1. INTRODUCTION

Radiometric characteristics of an imaging system describe how the system responds to various input radiance levels. The radiometric properties of the digital sensors are superior in comparison to those of the film sensors (Perko et al., 2004; Perko, 2005). The central radiometric properties of the film images are logarithmic response, typically 6 to 7 bit dynamic range, high image noise due to granularity, and poor stability (Boland et al., 2004; Graham et al., 2004). The film images have not been used extensively in quantitative remote sensing applications due to the complexity of their radiometry. The digital sensors can have linear radiometric response, 12 bit or even larger dynamic range, high radiometric resolution, low noise level, and good stability (Boland et al., 2004), and are thus appropriate for radiometric calibration. These radiometric properties enable the use of images in the classical photogrammetric tasks (e.g. automatic tie point measurement, feature extraction, DEM measurement), improve the automation level and quality of these tasks, and enable new application areas (e.g. change detection, classification) (Perko, 2005; Leberl and Gruber, 2005).

Many phenomena influence the image radiometry (Section 2.1). The practical consequence of this is that the same object provides different DN in different parts of a single image and in different images. The images should be either absolutely or relatively radiometrically referenced in order to quantitatively utilize the radiometric information. The optimum radiometric processing is dependent on the application; for digital photogrammetric instruments at least 3 types of applications are possible: visual applications, classical remote sensing applications that utilize normalized image data, and future remote sensing applications that utilize the anisotropic reflectance properties of the objects (bidirectional reflectance distribution function, BRDF). New methods are needed at photogrammetric production lines to process the image radiometry in a controlled way; the classical methods using antivignetting filters and statistical tonal balancing, used with film images, are not appropriate for digital sensors. Rigorous processing methods have been developed for the satellite images and for the airborne remote sensing instruments (e.g. Schowengerdt, 1997; Pellikka, 1998;

Liang, 2004; Atcor, 2007). Methods for photogrammetric sensors are also under development (Papadrotis et al., 2006; Beisl, 2006a; 2006b). For different sensors different processing steps are needed and support from sensor manufacturers is needed in development of the processing chains. Huge amounts of data are provided by photogrammetric techniques, thus the methods should be

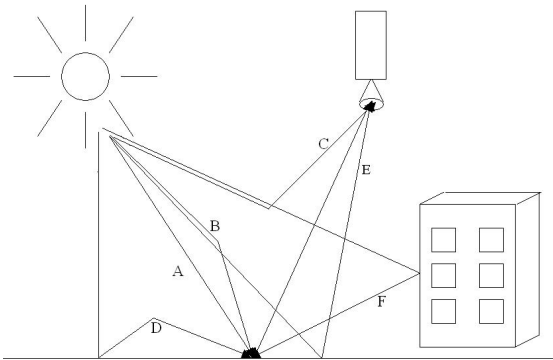


Fig 1. Radiation components in the wavelength range of 400-2500 nm (adopted from Beisl 2001).

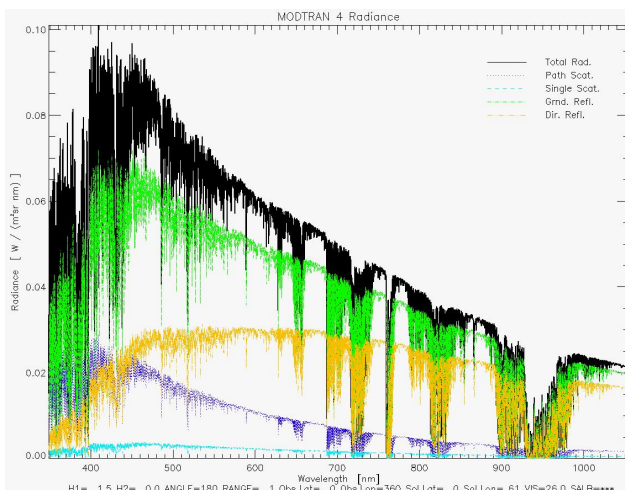
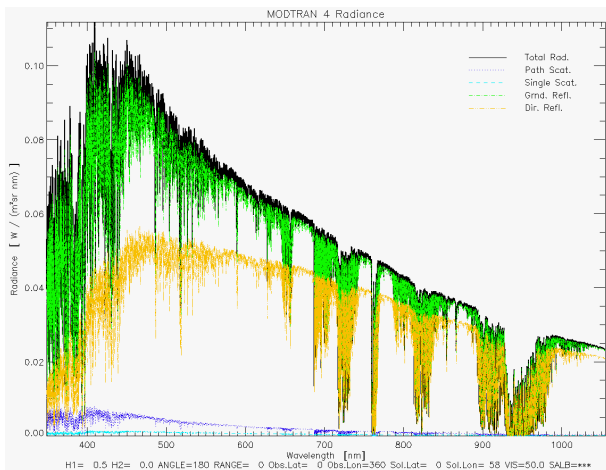


Fig 2. Radiation components for a 30% reflectance target provided by MODTRAN 4 as the function of the wavelength. Atmospheric model: midlatitude summer, rural. Top: Flying altitude 500 m, visibility 50 km. Bottom: Flying altitude 1520 m, visibility 26 km.

efficient.

Objective of this study is to evaluate empirically and from available literature the radiometric performance of four different photogrammetric imaging sensors. The tested sensors are the large-format sensors Leica Geosystems ADS40, Intergraph DMC, and Vexcel UltraCamD and the medium-format sensor Emerge DSS.

In Section 2 a brief review is made to image radiometry and the radiometric properties of the sensors under evaluation. The materials and methods are described in Section 3 and the results are given in Section 4. The discussion in Section 5 concludes this article.

2. RADIOMETRIC CHARACTERISTICS OF DIGITAL PHOTOGRAMMETRIC SENSORS

2.1. Image radiometry

The digital number (DN) output of the sensor is on the one hand dependent on the radiance entering the sensor and on the other hand on the sensor properties and settings.

The radiation components reaching the sensor (at-sensor radiance) are illustrated in Fig 1 (adopted from Beisl, 2001). They include the direct component (A), the skylight (B), the path-scattered radiance (C), the multiple scattering (D), the adjacency effect (E), and the illumination by reflected light (F). In good weather conditions the components A, B, and C are of importance. In Fig 2 MODTRAN 4 examples of the magnitudes of the most significant radiation components are given (A: Dir. Refl, A+B: Grnd. Refl, C: Path. Scat). The radiation components were calculated for the 30% reflectance target (Section 3.2.) for the conditions of the DMC (flying height $H=500$ m) and ADS40 ($H=1520$ m) missions (Section 3.1.). The magnitudes of various components are dependent on the sensor and system, land surface BRDF, atmosphere, topography, and temporal factors (Pellikka, 1998).

For the image interpretation applications the reflectance properties derived from the direct component (A) are of interest, while the other radiation components are disturbances that have to be eliminated. Most natural objects have anisotropic reflectance properties, which means that the object reflectance varies with respect to the direction of the illumination and observation (Lillesand and Kiefer, 2000; Beisl, 2001). The directional behavior of the object at a given wavelength is mathematically modeled using the Bidirectional Reflectance Distribution Function (BRDF). Anisotropic performance of the objects is of great interest for the quantitative analysis, while it disturbs visual applications, classical remote sensing methods utilizing normalized data, the generation of seamless orthophoto mosaics, etc. (Lillesand and Kiefer, 2000; Beisl, 2001; Liang, 2004).

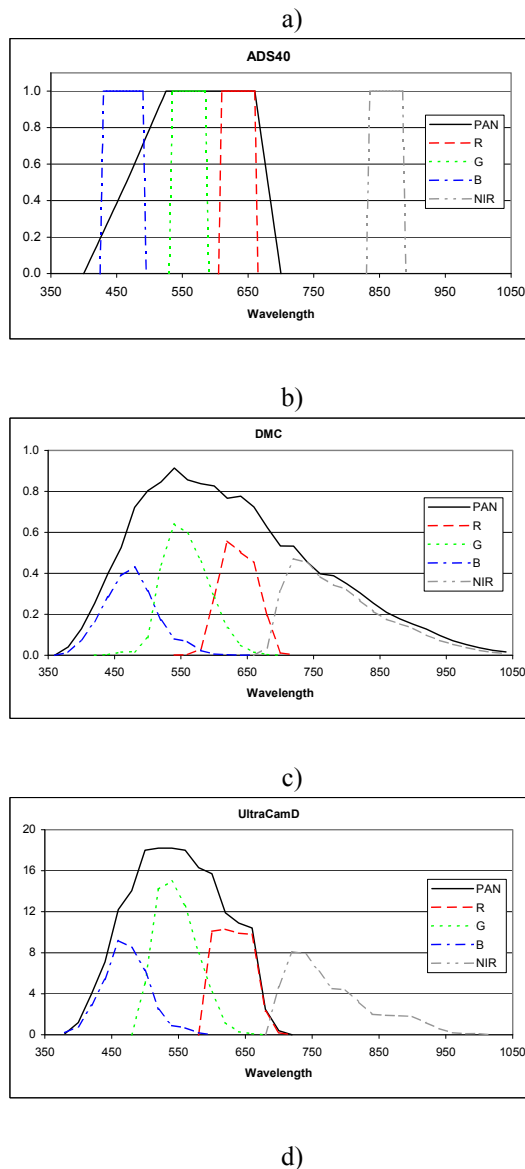
Important sensor properties influencing the recorded DNs are the spectral sensitivity, color formation principle, pixel depth, dynamic range (noise and saturation level), sensitivity, and lens quality (e.g. modulation transfer function, lens/system distortions, and chromatic aberrations). Important system settings controlling the amount of radiation are the aperture, integration time, and flying speed.

The sensor must be radiometrically calibrated in order to rigorously utilize the radiometry of the images. The quantities that should be calibrated are the DN nonuniformities, the spectral response, and the radiometric response. Furthermore, the calibration should ensure that the system meets the system specifications. Many factors cause DN nonuniformity; the most important ones are the light falloff caused by lens, filters, and aperture; sensitivity differences of individual CCD elements; errors of individual CCD elements; and effects of temperature (Beisl, 2006a; Hefele, 2006). The spectral calibration determines the locations and the shapes of the spectral bands (Schowengerdt, 1997; Beisl, 2006a). The absolute calibration determines the function, which is used to transform the DNs to units of radiance ($W/(m^2 sr^1 nm)$); for the CCD sensors typically the linear model is appropriate (Schowengerdt, 1997; Beisl, 2006a). The methods for the radiometric calibration are the laboratory, in-flight, and vicarious calibration.

2.2. Radiometric properties of digital photogrammetric sensors

Intergraph DMC (Hinz et al., 2000; Diener et al., 2000; Hefele, 2006) and Vexcel UltraCamD (Leberl and Gruber, 2003; 2005) are so called multihead large format sensors. These sensors provide the multispectral (MS) imagery by collecting red (R), green (G), blue (B), and near infrared (NIR) channels using individual cameras, and provide the large-format panchromatic image by combining several medium format images. Both the DMC and UltraCamD use DALSA CCD sensors having larger than 72 dB dynamic range (Dalsa, 2007). DMC occupies 3 k x 2 k DALSA FTF 3020M sensor for MS-channels, with 12 μm x 12 μm pixel size. UltraCamD use 4 k x 2.6 k DALSA FTF 4027M CCD array with 9 μm x 9 μm pixel size. The spectral channels of DMC and UltraCamD are wide (>200 nm) and overlapping (Fig 3b, c). The major difference of the sensors is that the spectral sensitivity of the DMC PAN channels extends to the NIR-area, while the UltraCamD PAN channel does not cover the NIR. The systems provide coarser spatial resolution for the MS-channels than for the PAN channel; the GSD reduction factor is 4.8 for DMC and 3.6 for UltraCamD. It is possible to improve the MS resolution by pansharping, which however is not typically recommended for the quantitative evaluations. The AD conversion of the UltraCamD is performed with 14 bits while the DMC applies 12 bit. Both systems apply electronic time delayed integration (TDI) based forward motion compensation (FMC).

ADS40 is a pushbroom sensor, which has single lens and individual lines for PAN, R, G, B, and NIR channels with 12000 pixels and 6.5 μm by 6.5 μm pixel size (Reulke et al., 2000; Sandau et al., 2000; Beisl, 2006a). The ADS40 spectral channels are similar to the IKONOS and Landsat TM channels, and are optimized for vegetation studies (Reulke et al., 2000). The spectral channels are narrow (approx. 50 nm), non-overlapping, and have steep edges (Fig 3a). The accurate interference



Radiometric Response: CIR Mode

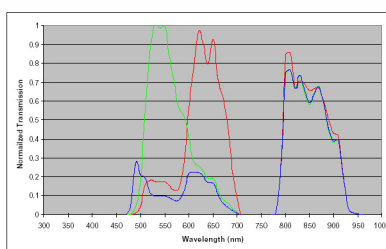


Fig 3. Spectral sensitivities of a) ADS40 (nominal values), b) DMC, c) UltraCamD, and d) DSS (CIR mode, Applanix 2007).

filters, trichroid beam splitter, telecentric lens, temperature stabilization of the focal plate, and the accurate radiometric calibration provide a reliable background for radiometric evaluations (Beisl, 2006a). Three multispectral channels (typically R, G, and B) are provided using a special trichroid beam splitter in order to obtain perfectly overlapping images.

In contrast to these large format sensors, the Emerge DSS provides medium sized 4000 x 4000 pixel image format (recently larger CCD chips have been implemented) (Mostafa and Hutton, 2005; Applanix 2007). The DSS provides 3 multispectral channels, R, G, and B or R, G, and NIR, using the Bayer matrix approach to separate various colors. The spectral channels are wide and overlapping (Fig 3d).

For the ADS40 the literature gives detailed description of the sensor radiometric properties, while for the DMC, UltraCamD, and DSS not as detailed description is given. For the ADS40 the absolute radiometric processing chain has been recently established (Beisl, 2006a; 2006b); the radiometric calibration of the DMC, UltraCamD, and DSS appears to concern the CCD sensor uniformity and light falloff.

Pros and cons of various sensors have been discussed in the literature recently. They include the color artifacts of the DMC and UltraCamD PAN-sharpened images; possible negative influences of the electronic TDI; color artifacts of the UltraCamD caused by the lens quality; problems and limitations in dynamic range of pushbroom sensors due to short integration times; unrealistic colorimetric content of the ADS40 caused by the separate spectral channels; displacement of one of the MS-channels of the ADS40; the reduced resolution and color artifacts of the mosaic filter approaches; chromatic aberrations of the DSS; missing FMC of the DSS (Fricker and Rohrbach 2005, Leberl and Gruber 2005, Pacey and Fricker 2005, and Souchon et al. 2006).

Table 1: Large format image materials (from Markelin et al., (2008)).

Sensor	DMC	DMC	ADS40	ADS40	UltraCamD	UltraCamD
Data set	d1_g5	d1_g8a	A1_g15	a1_g25	u4_g4	u4_g8
Date	1.9.2005	1.9.2005	26.9.2005	26.9.2005	5.7.2006	1.7.2006
Time (EET)	10:25-11:14	11:24-11:53	12:58-13:38	12:13-12:45	10:24-11:08	11:11-11:54
H (m)	500	800	1500	2500	480	940
GSD (cm)	PAN: 5 MS: 22	PAN: 8 MS: 38	PAN: 15 MS: 15	PAN: 25 MS: 25	PAN: 4 MS: 12	PAN: 8 MS: 24
V (m/s)	77	87	75	84	82	95
Exposure (ms)	PAN: 5.4-6.7 NIR: 5.4-6.7 RGB: 5.0-5.8	PAN: 5.6-5.7 NIR: 5.4-6.7 RGB: 4.7-4.8	1.65-2.0	2.6-3.1	4.0	4.0
Aperture	PAN: 11 MS N: 8.0 MS RGB: 5.6	PAN: 11 MS N: 8.0 MS RGB: 5.6	-	-	8	8
TDI steps	PAN: 34 MS: 7	PAN: 26 MS: 5	-	-	n/a	n/a
Visibility (km)	42	42	25	28	40	41
Solar zenith angle (°)	58.4	54.2	61.4	62	37.8	41.1
Solar azimuth (°)	137.2	154.4	180	167.5	192.3	142.7
Number of images	3	3	1	1	3	3

3. EXPERIMENTAL STUDY

3.1. Materials

Test flights with the ADS40, DMC, UltraCamD, and DSS were performed at the Sjökuulla test field (Fig 4) of the Finnish Geodetic Institute (FGI) (Honkavaara et al., 2008). The analysis of the data was described by Markelin et al. (2006; 2008). In this article some central results of the previous studies are given and further analysis is presented. Details of the large format image materials are given in Table 1.

The ADS40 test-flight took place in the end of September 2005. The Sun was approximately 30° above the horizon. The objective of the flight campaign was to test and characterize the new camera system of the Estonian Land Board. The sensor was installed in the Rockwell 690 Turbo Commander (OH-ACN) belonging to the National Land Survey of Finland (NLS). Data collected from 1500 and 2500 m flying heights were used. Weather and illumination conditions were acceptable for a photogrammetric mission.

The DMC test flights were performed in the beginning of September 2005. Data from test flights with 500 and 800 m flying heights were analyzed. Data was collected during midday with the sun angle of approximately 35° from horizon. The flight was performed using a rented camera and an experienced operator. The sensor was installed in the NLS Rockwell 690 Turbo Commander. Weather conditions during the mission were excellent.

The UltraCamD data was obtained from a regular calibration flight of a mapping company. Image blocks were collected from 480 and 940 m altitudes. The weather was slightly cloudy, but acceptable for photogrammetric mission. The survey aircraft was the Rockwell 690 Turbo Commander (OH-UTI) belonging to the Blom ASA. For the mission only four reflectance targets were available (5%, 25%, 45%, 70%).

The DSS mission was performed by Blom ASA at 12th and 14th of July 2005. Data from 1000 m and 3000 m flying heights was analyzed, resulting GSD's 16 cm and 50 cm, respectively. The aircraft was a Piper Navajo PA 31. DSS images were received from the company as 8-bits per channel CIR images. Details of the radiometric processing are not available, but it is assumed that the radiometric processing parameters were optimized for the visual inspection. This typically



Fig 4. Left: The Sjökulla image quality test field. Right: The reflectance reference targets (8-step gray scale).

means the clipping of the image histogram from the light and dark ends and nonlinear mapping from 16 bit to 12 bit DN domain.

In the cases of ADS40, DMC, and UltraCamD the raw images were evaluated. For the ADS40 images the laboratory determined radiometric corrections (Beisl, 2006a) were applied, while for the DMC and UltraCamD images not any corrections were applied. It can be assumed that the lacking corrections appear as increased noise for the DMC and UltraCamD, but does not influence analysis seriously, because only central

parts of the images were used. This approach was selected, because the processing of the images to the Level 3 caused changes for the DN dynamic range and channel ratios, which disturbs the analysis. In practice the laboratory calibration should be applied before the absolute calibration.

3.2. Methods

The approach for the system evaluation was to perform a radiometric test field calibration, which provides the system characterization and partially the sensor radiometric calibration. Accurate radiometric calibration requires careful design, preparation, and performance of the flight mission. The method is described in details by Honkavaara et al. (2008) and Markelin et al. (2008).

The FGI 8-step gray scale was used as the reflectance reference target (Fig 4; Honkavaara et al., 2008; Markelin et al., 2008). It consists of eight targets of size 5 m x 5 m. The target nominal reflectances are 5%, 10%, 20%, 25%, 30%, 45%, 50% and 70%. The targets were measured using the FiGIFiGo field goniometer of the FGI equipped with the ASD Field Spec Pro FR spectrometer at the laboratory under artificial light (Markelin et al., 2008). The properties of the targets are discussed by Markelin et al. (2008).

Atmospheric correction was performed by MODTRAN4 radiative transfer code (Version 3.1; Berk et al., 2003) using the MODO interface (Version 3.0.6; Schläpfer and Nieke, 2005). The default rural mid-latitude summer atmospheric model with the available visibility information (Table 1) was used, because atmospheric data was not collected at the test site during the missions. The at-sensor radiances for each band were obtained by propagating the laboratory determined target nadir spectral profiles through the modeled atmosphere and integrating over the sensor spectral sensitivities (Fig 3). The radiation components for the 30% reflectance targets for the DMC (H=500 m) and ADS40 (H=1500 m) are shown in Fig 2. Because the full target BRDF was not available, only the images where the gray scale was located close to the image nadir were evaluated.

For each reflectance target the DN statistics (average, minimum, maximum, standard deviation) were calculated on image windows corresponding 2 m x 2 m area at object space. The average DN's were evaluated as the function of the at-sensor radiances. The maximum and minimum values of image histograms were used to support the dynamic range analysis.

The 8-step gray scale of the FGI enables the determination of the sensor radiometric response, dynamic range, absolute calibration, and sensitivity. Due to the limitations of the study (lacking insitu reflectance and atmospheric measurements) the results of the first two issues can be considered reliable, while the rest should be considered as indicative.

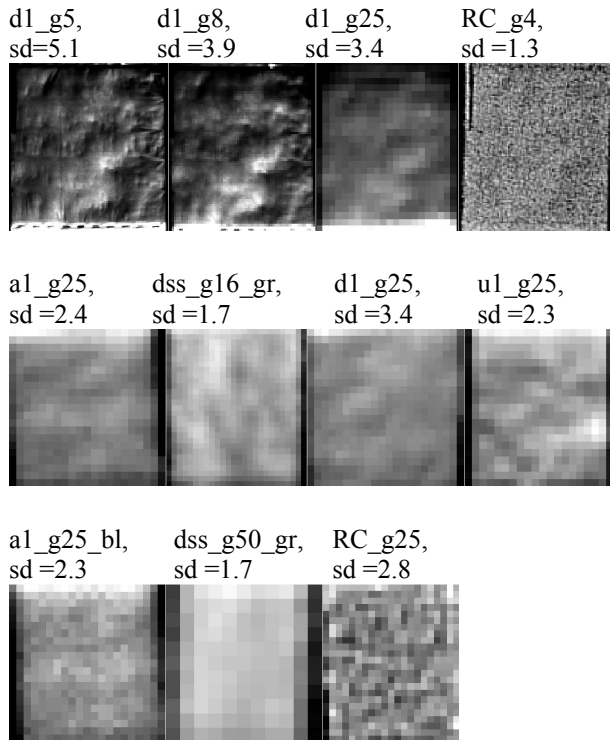


Fig 5. Examples of the 30% target. Standard deviation (sd) of the target is shown as percentage of the gray value. Sensors: ADS40 (a1), DMC (d1), UltraCamDD (u1), DSS (dss), RC20 (RC). The number after _g shows the GSD in cm. gr: green channel, bl: blue channel, other examples are from panchromatic images.

Table 2. Histogram statistics of the large format data sets. Minimum and maximum DN's and the DN range in bits (DR).

		d1_g5	d1_g8	a1_g15	a1_g25	u4_g4	u4_g8
P	min	67	0	312	649	251	360
	max	4095	4095	7175	8369	6791	6866
N	DR (bit)	12.0	12.0	12.7	12.9	12.7	12.7
R	min	0	0	15	52	197	214
	max	4095	4095	1064	1413	6441	6653
	DR (bit)	12.0	12.0	10.0	10.4	12.6	12.7
G	min	33	42	13	58	209	244
	max	4095	4095	1025	1222	6552	6663
	DR (bit)	12.0	12.0	10.0	10.2	12.6	12.6
B	min	34	45	32	95	182	213
	max	4095	4095	641	814	6445	6535
	DR (bit)	12.0	12.0	9.3	9.5	12.6	12.6
N	min	0	0	14	57	293	340
	max	4095	4095	1723	2171	6321	6467
R	DR (bit)	12.0	12.0	10.7	11.0	12.6	12.6

Each channel use similar CCD-line, thus the lower sensitivity of the MS-channels in comparison to the PAN channels is caused by the narrow spectral filters. The reason for the lower sensitivity of the

4. RESULTS AND DISCUSSION

Examples of the gray scale and the radiometric response plots (DN as the function of the at-sensor radiance) are shown in Fig 7 to Fig 10. In Table 2 the histogram statistics of entire images are given.

In Fig 5 examples of DMC, UltraCamD, ADS40, DSS, and RC20 images of the stretched 30% reflectance target are shown to illustrate the radiometric resolution and noise of various sensors. The targets, made of flexible material, are laid on rough terrain, which causes topo-graphic differences visible on images. The target topography is clearly visible on digital images, while on analog images mainly noise caused by granularity appears. For film images 1.3% and 2.8% standard deviations correspond well with the noise expectations (e.g. Kölbl, 2005).

4.1. ADS40

The ADS40 results are shown in Fig 6 and Table 2. The problem with the ADS40 was that the photogrammetric recording mode was used. This mode compresses small batches of data to 8 bit/pixel domain and further JPEG-compresses the data (Beisl, 2006b). This caused artifacts (“striping”) for the 2-3 brightest targets (Fig 6a), because the mode was not able to accurately compress the data having very bright (target reflectance > 45%) and very dark values (background reflectance approx. 5%).

The linearity of the sensor radiometric response was good for the five darkest targets (Fig 6b); the non-linearity of the 3rd target is explained in Section 4.2.

Various channels showed substantially different DN dynamic range (Table 2). The DN dynamic range of the panchromatic channel appeared to be close to 13 bits while the DN dynamic ranges of the MS-channels were 10, 10, 9, and 11 bit for red, green, blue, and NIR channels, respectively.

The different dynamic ranges were caused by different sensitivities of various channels.

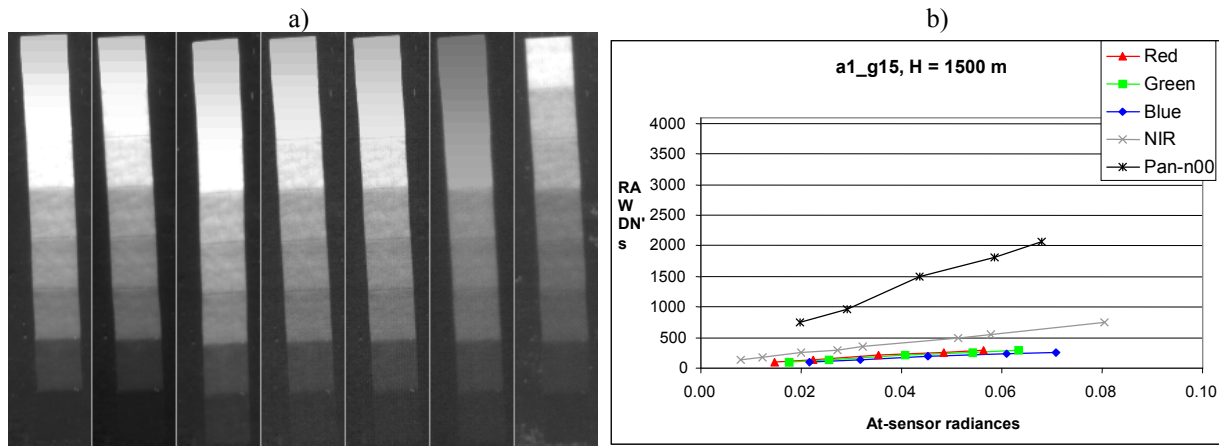


Fig 6. ADS40 radiometric analysis (GSD: PAN and MS: 15 cm). a) Channels from left to right: pan-b14, pan-n0, pan-f28, red-f16, green-f16, blue-f16, nir-b02 (letters and numbers show the direction of the line, i.e. b: backward, n: nadir, f: forward; e.g. f28: 28 degrees forward). b) Radiometric response plot.

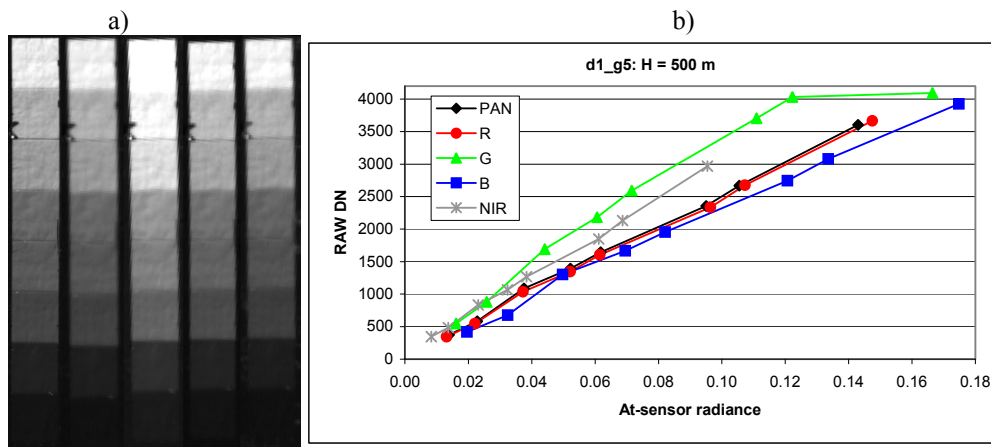


Fig 7. DMC radiometric analysis (GSD: PAN: 5 cm, MS: 22 cm.). a) From left to right: PAN, R, G, B, NIR. b) Radiometric response plot.

R, G, and B channels in comparison to the NIR-channel was the energy reduction caused by the trichroid beam splitter. The dynamic range was slightly better for the 25 cm GSD than for the 15cm GSD due to the relatively longer integration times. In Fig 5 the lower dynamic range of the blue channel appeared visually as lower radiometric resolution in comparison to the panchromatic image.

4.2. DMC

The radiometric response plot (Fig 7) showed that the DMC radiometric response was linear; the nonlinearity of the green channel at the brightest targets was caused by the saturation due to overexposure.

The image histograms (Table 2) showed that the DMC utilized the 12-bit dynamic range entirely. The sensitivity of the PAN, red, and blue channels appeared to be similar, while the green and NIR-channels appeared to be more sensitive (Fig 7). The sensitivity of the green channel was a problem, because the data was saturated with greater than 45% object reflectance.

Absolute calibration results of the DMC are shown in Table 3. The full linear model was needed only for the NIR-channel. The accuracy of the absolute calibration was evaluated by using 5% and 70% targets as the reference and the remaining targets for checking (for the green channel 5% and 50% targets were used as reference because of the saturation of the green channel). The results (Fig

Table 3. Absolute calibration parameters for the DMC (d1_g5), s0 is the standard error of unit weight.

Band	param.		Stdev		s0 W/(m ² sr nm)
	cal gain	offset	cal gain	offset	
PAN	2.54E-04	-	2.76E-06	-	1.75E-03
R	2.09E-04	-	2.13E-06	-	1.65E-03
G	1.55E-04	-	2.74E-06	-	2.85E-03
B	2.36E-04	-	2.78E-06	-	2.12E-03
NIR	2.16E-04	-4.69E-03	3.30E-06	8.41E-04	2.34E-03

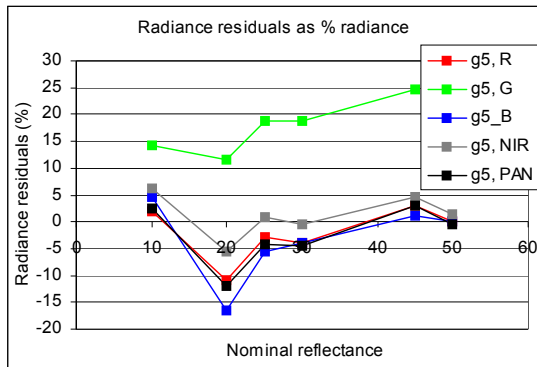


Fig 8. Residuals of the absolute calibration.

of the UltraCamD appeared to be up to 12.7 bit (Table 2).

The sensitivity of the red and NIR channels appeared to be fairly similar, while the green channel was slightly less sensitive (Fig 9). The blue channel was clearly the least sensitive and the panchromatic channel was the most sensitive.

The results of two flying heights were similar with an exception that at the 800 m flying height the red and panchromatic channels saturated at the brightest targets.

4.4. DSS

For the DSS the DNs are plotted as the function of reflectance (Fig 10), thus this evaluation gives possibility to evaluate the saturation and the linearity. An additional difference is that for the DSS the pixel depth was 8-bit for each channel and the radiometric processing method was unknown. The radiometric response appeared to be linear for 5%, 10%, and 25% targets, but the images began to saturate already at reflectances greater than 25%. The radiometric resolution and noise of the 8-bit/channel images appeared to outperform those of the film data (Fig 5).

5. DISCUSSION AND CONCLUSIONS

The radiometric performance of the large format photogrammetric sensors ADS40, DMC, and UltraCamD, and the medium format sensor DSS were evaluated using a 8-step gray scale. The radiometric evaluations showed that ADS40, DMC, and UltraCamD provided excellent radiometric quality that can be absolutely calibrated. The results quantitatively proved the linear radiometric response and large, up to 13-bit DN dynamic range. Also the excellent radiometric resolution and low noise level were apparent. Detected problems included the danger of overexposure of UltraCamD and DMC and in contrary, the low sensitivity of the ADS40 multispectral channels. Analysis of DSS was not as detailed as the analysis of the other sensors.

8) indicated that the reference value for the 20% target was an outlier. The calibration accuracy of the green channel appeared to be weaker than the accuracy of the other channels. The reason for this was that the 50% target was already slightly saturated. When leaving out these two suspected outliers from the analysis, the relative calibration accuracy (RMSE) was 3%; the major error component was the reference reflectance inaccuracy. Additional error source is the atmospheric correction, which could not be evaluated in this study.

Results were similar for the 500 m and 800 m flying heights.

4.3. UltraCamD

For the UltraCamD mission only four reflectance targets were available (5%, 25%, 45%, 70%). The results indicated good linearity (Fig 9). The dynamic range

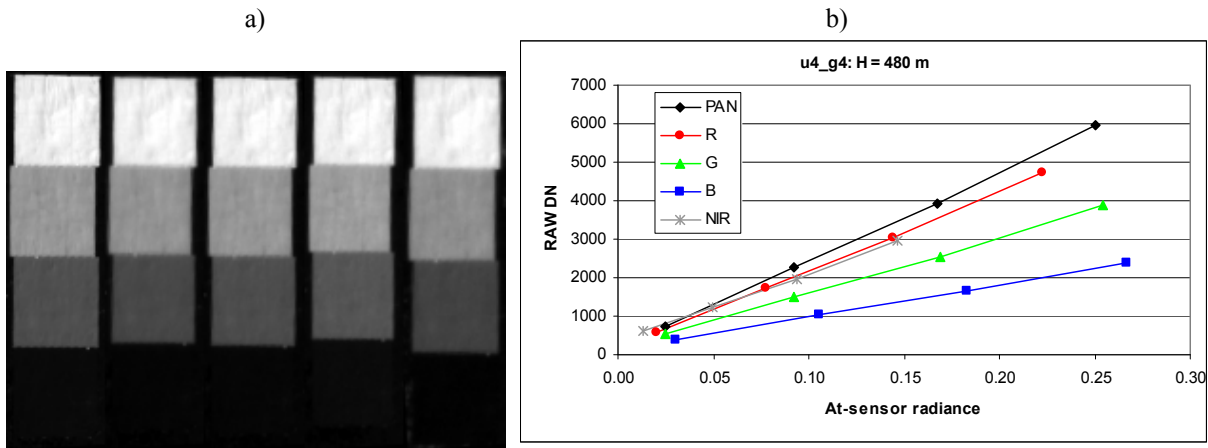


Fig 9. UltraCamD radiometric analysis (GSD: PAN: 4 cm, MS: 12 cm). a) Channels from left to right: PAN, R, G, B, NIR. b) Radiometric response plot.

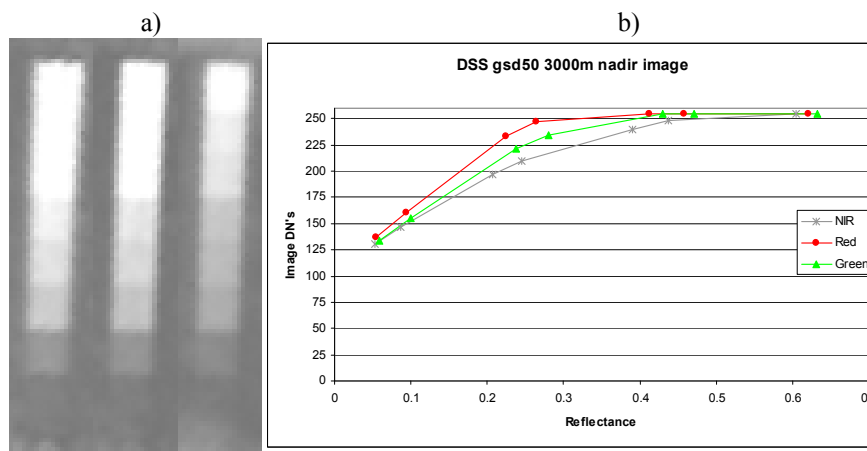


Fig 10. DSS radiometric analysis, GSD=50 cm. a) Channels from left to right: R, G, NIR. b) DN's plotted as the function of the reflectance.

Several pros and cons of various sensors were summarized in the article, which should be taken into account when selecting sensors for particular mapping applications. In the future the effects of these factors should be studied both by simulations and empirically.

The primary method for the radiometric calibration should be the laboratory calibration, where the effects of all the influencing factors (aperture, temperature, exposure, etc.) can be systematically evaluated. The accurate calibration on the single pixel level is possible only in laboratory. It is essential also to perform test field calibration to find out the performance of the entire system. For instance, this study showed that the ADS40, combined with the relatively high-speed aircraft, was probably not the optimal system for the Finnish illumination conditions. The DMC and UltraCamD indicated sensitivity on aperture and exposure time settings and the risk of overexposure, which has to be taken into account when collecting data for quantitative evaluations. Also the system MTF and geometric properties (lens distortions, image distortions) should be determined in airborne conditions to ensure the highest radiometric quality.

There exist 2nd generation ADS40 (Leica Geosystems, 2007) and UltraCam (Vexcel, 2007: UltraCamX) sensors. For the 2nd generation sensors several shortcomings of the 1st generation sensors, detected in this and some other studies, have been improved. Central radiometric changes of the ADS40 sensor include the 4 times better sensitivity, wider spectral filters, and tetrachroid beam splitter to provide perfect alignment of all four multispectral channels. For the UltraCamX the

reported improvements include the better lens, the increased CCD array sizes, and improved PAN-sharpening ratio.

A demanding task is the operational radiometric correction of every collected image flight. Functional methods for the relative and absolute radiometric correction are central research topics in the future. Whatever the radiometric processing function is, the traceability to the original raw DN's (or the original data itself) should be maintained in order to ensure the quantitative use of the data in the future.

6. ACKNOWLEDGEMENTS

Efforts of several companies and persons made this study possible. FGI performed the DMC mission in co-operation with the National Land Survey of Finland (NLS). The UltraCamD mission was a co-operation project of FM-Kartta Ltd, FGI and NLS. The ADS40 campaign was performed in co-operation with Estonian Land Board, FGI and NLS. Efforts and valuable comments of these companies and authorities are gratefully acknowledged. Assistance of several individuals at the FGI is appreciated.

7. REFERENCES

- Applanix, 2007. <http://www.applanix.com> (Last date accessed 28 June 2007).
- Atcor, 2007. <http://www.rese.ch/atcor/index.html> (Last date accessed 28 June 2007).
- Beisl, U., 2001. Correction of bidirectional effects in imaging spectrometer data. Remote Sensing Series 27, Remote Sensing Laboratories, Department of Geography, University of Zurich, 2001.
- Beisl, U., 2006a. Absolute spectroradiometric calibration of the ADS40 sensor, International Archives of Photogrammetry, Remote Sensing and Spatial Information Sciences, 36 (B1), on CD-ROM, 5 pages.
- Beisl, U., 2006b. Absolute spectroradiometric calibration of the ADS40 sensor, Presentation given at ISPRS Comm. I Symposium in Paris, July 2006, 21 pages.
- Berk, A., G. Anderson, P. Acharya, M. Hoke, J. Chetwynd, L. Bernstein, E. Shettle, M. Matthew and S. Alder-Golden, 2003. MODTRAN4 Version 3 Revision 1 User's Manual, Air Force Research Laboratory, Space Vehicles Directorate, Hanscom Air Force Base, Ma 01731-3010, 101 p.
- Boland, J., T. Ager, E. Edwards, E. Frey, P. Jones, R.K. Jungquiet, A.G. Lareau, J. Lebaron, C.S. King, K. Komazaki, C. Toth, S. Walker, E. Whittaker, P. Zavattono and H. Zuegge, 2004. Cameras and sensing systems, ASPRS Manual of Photogrammetry, 5th Edition, (J. C. McGlone, E. Mikhail, J. Bethel, editors), American Society for Photogrammetry and Remote Sensing, pp. 581-676.
- Dalsa, 2006. Dalsa Professional Imaging, <http://www.dalsa.com/pi/index.asp> (last date accessed: 28 June 2007).

- Diener, S., M. Kiefner and C. Dörstel, 2000. Radiometric normalisation and colour composite generation of the DMC, *International Archives of Photogrammetry and Remote Sensing*, 33(1), pp. 82-88.
- Fricker, P. and A. Rohrbach, 2005. Pushbroom scanner provide highest resolution earth imaging information in multispectral bands. *Proceedings of the ISPRS Hannover Workshop, 17-20 May 2005, CD-ROM*, 5 p.
- Graham, R., A. Koh, M. Baltsavias, M. v. Schönemark, A.J.P. Theuwissen, H. Ziemann, 2004. Detectors and sensors, *ASPRS Manual of Photogrammetry, 5th Edition*, (J. C. McGlone, E. Mikhail, J. Bethel, editors), American Society for Photogrammetry and Remote Sensing, pp. 505-580.
- Hefele, J., 2006. Calibration experience with the DMC, *Proceedings of EuroSDR Commission I and ISPRS Working Group 1/3 Workshop EuroCOW, 25-27 January 2006, CD-ROM*, 6 p.
- Hinz A., C. Dörstel and H. Heier, 2000. Digital Modular Camera: System Concept and Data Processing Workflow, *International Archives of Photogrammetry and Remote Sensing*, 33, 6p.
- Honkavaara, E., J. Peltoniemi, E. Ahokas, R. Kuittinen, J. Hyypä, J. Jaakkola, H. Kaartinen, L. Markelin, K. Nurminen and J. Suomalainen, 2008. A permanent test field for digital photogrammetric systems, *Photogrammetric Engineering & Remote Sensing*, In press.
- Kölbl, O., 2005. Transfer functions in image data collection. In: Fritsch (ed.), *Proceedings of the 50th Photogrammetric Week 2005*, Wichmann Verlag, pp. 93-104.
- Leberl, F. and M. Gruber, 2003. Flying the new large format digital aerial camera Ultracam. In: Fritsch (ed.), *Proceedings of the 49th Photogrammetric Week 2003*, Wichmann Verlag, pp. 67-76.
- Leberl, F. and M. Gruber, 2005. UltraCamD: Understanding some noteworthy capabilities. In: Fritsch (ed.), *Proceedings of the 50th Photogrammetric Week 2005*, Wichmann Verlag, pp. 57-68.
- Leica Geosystems, 2006. ADS40 2nd Generation datasheet. URL: <http://www.leica-geosystems.com/> (last date accessed: 28 June 2007).
- Liang, S., 2004. *Quantitative remote sensing of land surfaces*. John Wiley & Sons, Inc.
- Lillesand, T., R., Kiefer, 2000. *Remote sensing and image interpretation – 4th ed.* John Wiley & Sons, Inc.
- Markelin, L., E. Honkavaara, J. Peltoniemi, J. Suomalainen, and E. Ahokas, 2006. Radiometric evaluation of digital aerial cameras, *International Archives of Photogrammetry, Remote Sensing and Spatial Information Sciences*, 36 (B1), CD-ROM, 6 pages.
- Markelin, L., E. Honkavaara, J. Peltoniemi, E. Ahokas, J. Hyypä, R. Kuittinen, J. Suomalainen, 2008. Radiometric calibration and characterization of large-format digital photogrammetric sensors in a test field. *Photogrammetric Engineering & Remote Sensing*. In press.

- Mostafa, M.R. and J. Hutton, 2005. A fully integrated solution for aerial surveys: Design, development, and performance analysis. *Photogrammetric Engineering & Remote Sensing*, 75(4): pp. 391-398.
- Pacey, R. and P. Fricker, 2005. Forward motion compensation (FMC) – Is it the same in the digital imaging world, *Photogrammetric engineering & Remote Sensing*, 71(11): pp. 1241-1242.
- Paparoditis, N., J.-P. Souchon, G. Martinoty, and M. Pierrot-Deseilligny, 2006. High-end digital cameras and their impact on the automation and quality of the production workflow, *ISPRS Journal of Photogrammetry & Remote Sensing*, 60(6): pp. 400-412.
- Perko, R., A. Klaus, M. Gruber, 2004. Quality comparison of digital and film-based images for photogrammetric purposes. *International Archives of Photogrammetry, Remote Sensing and Spatial Information Sciences*, 35 (B1), pp. 1136-1140.
- Perko, R., 2005. Image quality: digital pansharpening versus full color film. Manuscript URL: <http://www.vexcel.co.at> (last date accessed 28 June 2007)
- Pellikka, P., 1998. Development of correction chain for multispectral airborne video data for natural resource assessment. *Fennia*, 176: p. 1.
- Sandau, R., B. Braunecker, H. Driescher, A. Eckardt, S. Hilbert, J. Hutton, W. Kirchhofer, E. Lithopoulos, R. Reulke and S. Wicki, 2000. Design principles of the LH Systems ADS40 Airborne Digital Sensor, *International Archives of Photogrammetry and Remote Sensing*, 33(1): pp. 258-265.
- Schläpfer, D., J. Nieke, 2005. Operational simulation of at sensor radiance sensitivity using the MODO/MODTRAN4 environment, *Proceedings of the 4th EARSeL Workshop on Imaging Spectroscopy*, Warsaw 2005.
- Schowengerdt, R.A., 1997. *Remote Sensing, models and methods for image processing*, Academic Press, USA, San Diego.
- Souchon, J.-P., N. Paparoditis, O. Martin, C. Meynard and C. Thom, 2006. Is there an ideal digital aerial camera? *International Archives of Photogrammetry, Remote Sensing and Spatial Information Sciences*, 36(A1), 6 p.
- Vexcel, 2007. <http://www.vexcel.com/> (Last date accessed: 28 June 2007)